Highly Sensitive D-Shaped Photonic Crystal Fiber-Based Plasmonic Biosensor in Visible to Near-IR

Ahmmed A. Rifat, Rajib Ahmed, G. Amouzad Mahdiraji, and F. R. Mahamd Adikan

***Abstract*— A simple D-shaped photonic crystal fiber (PCF)-based surface plasmon resonance (SPR) biosensor is proposed for refractive index sensing in visible to near infrared (IR) region. A thin Titanium di-oxide (TiO_2) layer is used as an adhesive layer to strongly attach the plasmonic gold (Au) layer with silica fiber surface. TiO_2 also helps to tune the operating sensor wavelength from visible to near IR (550–1770-nm wavelength). Finite-element method has been used to investigate the guiding properties. The proposed sensor shows the maximum wavelength interrogation sensitivity of 46 000 nm/RIU and the average sensitivity of 9,800 nm/RIU in the sensing range of 1.33–1.43. It also shows the maximum amplitude sensitivity of 1,086 RIU^{-1}. Using the wavelength and amplitude interrogation methods, proposed sensor gives the theoretical maximum resolution of 2.2×10^{-6} and 9.2×10^{-6} RIU, respectively. To the best of our knowledge, it has the highest sensitivity and sensor resolution among the reported PCF SPR sensors. The proposed D-shaped PCF has been fabricated following the standard stack-and-draw method to show the feasibility of the proposed sensor. Due to the promising results over the broad range of analyte RI, it would be an excellent candidate for the detection of biomolecules, organic chemicals, chemical, and other analytes.**

***Index Terms*— Photonic crystal fiber, surface plasmon resonance, optical fiber sensors.**

I. Introduction

In RECENT years, remarkable efforts have been made on photonic crystal fiber (PCF) based surface plasmon resonance (SPR) sensors due to its wide range of applications ranging from medical diagnostics, biochemical, environmental monitoring, and food safety to security [1]–[3]. PCFs can overcome the difficulties associated with the conventional prism based SPR sensors. In prism based SPR sensor, prism is coated with plasmonic materials (Ag, Au, Cu, etc.) and light is incident through the prism to excite the free electrons on metal surface. At a specific angle when the frequency of incident light and the metal surface electrons are matched, the electrons start to resonate, as a result surface plasmon wave (SPW) is generated and propagated along the metal-dielectric interface. Prism SPR sensors require light to be launched at a specific angle. Moreover, it require several mechanical (moving) components which lead to a bulky construction. Also, it has limitations on the remote sensing applications. [4], [5]. On the contrary, PCF is compact, light-weight and metal can be coated on either inside the air-holes or outside the fiber surface, resulting in the miniaturization of the sensor structure. Incident light can be simply launched from one end of the fiber and response can be observed from another fiber end. Moreover, propagating light can be controlled by changing the PCFs parameters such as air hole size, pitch size, pressurization and etc. during the fabrication process. By changing applied pressure on PCFs' holes, the air-hole diameters, pitch size, and the glass wall thickness between adjacent air-holes can be changed, thereby, the light penetration from the core to the cladding region changes [6]–[8]. By controlling the light propagation, strong coupling between the core mode and surface plasmon polaritons (spp) mode can be achieved, consequently improving the sensors performance [9], [10].

To date, numerous PCF SPR sensors have been reported which can be classified into five categories such as internal metal coated [9], [11], nanowire based [12]–[14], microfluidic slotted based [10], [15], external sensing approaches [16], [17] and D-shaped [18]–[20]. Internal metal coated and nanowire based PCF SPR sensors fabrication is quite difficult due to the requirement to coat or infiltrate liquid into the small air-holes surface. These fibers suffer huge propagation loss as the metal layers are selectively placed surrounding the core. The plasmonic metal surfaces attract the core field resulting in an increase in loss. Although microfluidic slotted based PCF SPR sensors have outside metal coating, but owing to its splitting specification on the external surface of PCF, the sensor implementation becomes complicated. The reported external PCF SPR sensor approaches are flexible in terms of fabrication. However, these sensors were accompanied either with one or two air hole rings which leads to the high propagation loss. This resulted in a complication in the practical realization of the PCF SPR sensors [10], [21]. Furthermore, these reported PCF SPR sensors required metal coating inside the air holes or outside the circular fiber structure, except the

Manuscript received January 21, 2017; accepted February 27, 2017. Date of publication March 3, 2017; date of current version April 10, 2017. This work was supported by the University of Malaya MOHE-High Impact Research under Grant UM.0000005/HIR.C1. The associate editor coordinating the review of this paper and approving it for publication was Dr. Carlos R. Zamarreno. *(Corresponding author: Ahmmed A. Rifat.)*

A. A. Rifat is with the Integrated Lightwave Research Group, Faculty of Engineering, University of Malaya, Kuala Lumpur 50603, Malaysia, and also with the Department of Electrical, Electronic and Telecommunication Engineering, BCMC College of Engineering and Technology, Jessore-7400, Bangladesh (e-mail: rifat.ahmmed@osamember.org).

R. Ahmed is with the School of Engineering, University of Birmingham, Birmingham B15 2TT, U.K. (e-mail: rajib.ahmed.apece@gmail.com).

G. A. Mahdiraji is with the Faculty of Engineering, Taylor's University, Subang Jaya 47500, Malaysia, and also with Flexilicate Sdn. Bhd., University of Malaya, Kuala Lumpur 50603, Malaysia (e-mail: ghafouram@gmail.com).

F. R. Mahamd Adikan is with the Integrated Lightwave Research Group, Faculty of Engineering, University of Malaya, Kuala Lumpur 50603, Malaysia, and also with Flexilicate Sdn. Bhd., University of Malaya, Kuala Lumpur 50603, Malaysia (e-mail: rafiq@um.edu.my).

Digital Object Identifier 10.1109/JSEN.2017.2677473

D-shaped sensors. Metal coating on circular fiber surface is another fabrication issue especially for uniform coating thickness and roughness [22]. Conventional metal coating methods such as RF sputtering, thermal evaporation methods, electrolysis plating or wet-chemistry deposition creates the massive surface roughness in the coating of circular surfaces [22], [23]. Chemical vapor deposition (CVD) method was also reported as a possible coating method in a circular surface, although it involves complex organometallic chemistry [24]. However, D-shaped as a flat surface, enhances the homogeneous metal coating possibilities with standard metal deposition methods. In order to characterize and utilize the sensor, self-calibration procedure is needed. Due to the flatness of the surface, sample liquids can be easily exchanged by using the water flow or by purging nitrogen gas through the surface [22]. Due to flat and outside metal coating, unknown analyte/sample could be detected by simply flowing through the metal surface [25].

Currently, several D-shaped PCF SPR sensors have been reported. D-shaped PCFs are formed by side polishing or etching one part of the PCF. D-shaped PCFs have flat surfaces where plasmonic metal layers can be coated easily. Tian *et al.* [26] first reported the solid core D-shaped PCF SPR sensor where 1st ring of the PCFs were scaled down to make the strong coupling between core and spp mode, the refractive index sensitivity was 7,300 nm/RIU and the figure of merits (FOMs) which is the ratio of spectral sensitivity and full-width-half-maximum (FWHM) of the loss spectrum, is numerically calculated as 216 RIU^{-1}. Hollow core D-shaped PCF has been reported with liquid mixture filled in the core to improve the sensitivity [20]. It achieved the maximum sensitivity of 6,430 nm/RIU. Phase modulation behavior in SPR had also been studied in solid core D-shaped PCF structure by Tan *et al.* [27]. Recently, rectangular lattice [28] and square lattice [29] based D-shaped microstructure fiber has been reported and they achieved the sensitivity of 7,481 and 12,450 nm/RIU, respectively. Propagation loss of these rectangular and square lattice based D-shaped PCFs are 300 dB/cm and 6000 dB/m, respectively at analyte RI 1.38. Graphene on Silver based D-shaped SPR sensor were also reported to improve the performance [18], and achieved the maximum sensitivity of 3700 nm/RIU, theoretical sensor resolution of 2.7×10^{-5} RIU and propagation loss of 167 dB/cm. These reported D-shaped PCF SPR sensors were operating in the visible range. Recently, ITO based D-shaped SPR has been reported to switch the sensor operating wavelength to near-IR region [5]. However, besides the coating problem, propagation loss poses another important issue for practical realization of PCF SPR sensors. Although D-shaped fiber has the opportunity to reduce the propagation loss as its core is surrounded with the several rings and only one part is polished, but the reported D-shaped fiber showed high propagation loss which voids the practical realization. In practice, due to large propagation loss, input light will be attenuated immediately after it enters. It is not possible to generate a measurable signal at the output side to detect the sample. High fiber loss limits the fiber length to observe the sensor behavior. Due to the small length of sample PCF, it is required to align or splice with conventional single mode fiber (SMF). Very recently, using the commercial PCF parameters (LMA 31, NKT Photonics), low loss D-shaped PCF SPR sensor has been modeled , where the loss value showed 2.2 dB/m at 1,688 nm wavelength. However, it shows the moderate sensor sensitivity 5,200 nm/RIU, with the minimum sensor resolution of 1.92×10^{-5} RIU. For the accurate sample detection, high sensitivity with high sensor resolution is highly desirable, preferred but extremely challenging.

In this paper, we propose a highly sensitive, low loss D-shaped PCF based SPR sensor with operating wavelength in visible to near IR region. Operating wavelength visible to near IR wavelength makes this sensor more promising as it will find significant applications in the field of biomedical at near IR region. At near IR wavelengths, penetration depth of evanescent field is high, compared to the visible region. As a result a very sharp depth appears which enables the easier sensing detection [5], [30]. Furthermore, laser sources are commercially available at near IR region. Recently, it has been reported that the operating wavelength in near IR region using TiO_2 layer based PCF SPR sensor has been tuned [11], [25]. Proposed sensor performance is critically investigated based on wavelength interrogation (WI) and amplitude interrogation (AI) methods. Furthermore, the investigation rationally shows the fabrication tolerance such as the effects of air-holes diameter, pitch, gold thickness, TiO_2 thickness and polishing depth on the proposed sensor.

II. Design and Theoritical Modeling of D-Shaped PCF SPR Sensor

Figures 1(a) and (b) shows the schematic diagram of the proposed sensor in 3D view and cross-section view, respectively. Proposed D-shaped PCF could be realized by following the standard stack-and-fiber drawing method [6]. We have considered the commercially available capillary with outer diameter 25 mm and inner diameter 17.5 mm. As a result, we calculated the air-hole diameter is, $d = 4.69$ μm. We have taken the 6 rings PCF which helps to reduce the propagation loss, as the number of rings reduces the leaky modes. Top side of the PCF air holes are removed to form the D-shape and the polishing depth is $h = 8$ μm. The first ring air-holes are scaled down except the besides air-holes of the core to create the birefringent effects. Birefringent behavior makes the coupling to be stronger between the x-polarization or y-polarization core mode and spp mode. As a result of this, sensor performance is improved. Moreover, the upper row of the air holes from the core is also scaled down to reduce the gap between the core and sensing media. The evanescent field can easily hit on the metal surface and create a strong coupling effect between the core and spp mode. The scaled down air hole diameter is, $d_s = 3.28$ μm which can easily be achieved by one time jacketing of air hole, d with the same size capillary. A small air hole is considered in the center of the core which helps to spread the electric fields toward the surface. Small air hole diameter size is $d_c = 2.3$ μm which can be realized by two times jacketing of air hole, d with the same size capillary.

Hole to hole distance or pitch size is $\Lambda = 6.73$ μm. Plasmonic material gold layer is used on the flat surface of the fiber structure with thickness $t_g = 40$ nm. Also a thin

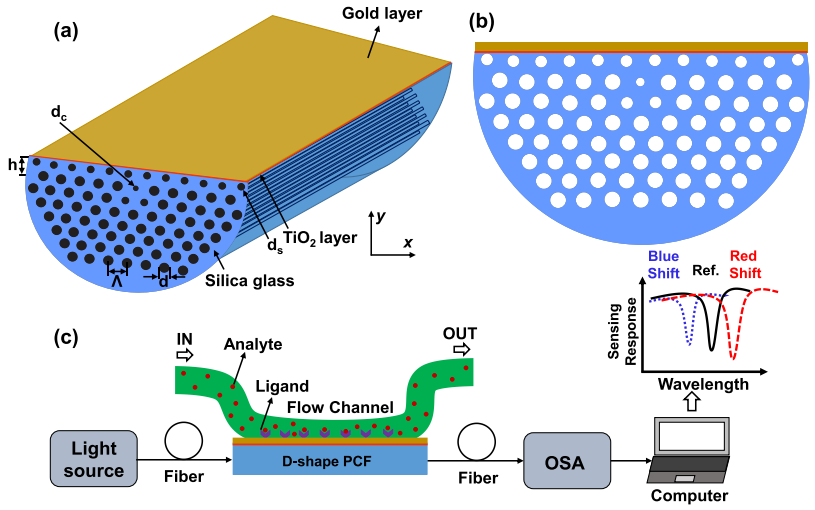

Fig. 1. Design structure. (a) Schematic diagram of the proposed D-shaped PCF SPR sensor in 3D model. (b) Cross-section of the computational structure. (c) Schematic diagram of the proposed sensor set-up.

TiO_2 layer with thickness $t_t = 5$ nm is considered as an adhesive layer between the flat surface and the gold layer. Gold and TiO_2 layer coating on the flat surface could be possible by CVD process. Sensing medium (defined with dielectric constant) where the sample will be placed or allowed to flow top of the gold surface. Background material silica refractive index has been adopted from the Sellmeier equation [9].

The dielectric constant of gold is defined by the Drude-Lorentz model [31] and the equation is,

$$\varepsilon_{Au} = \varepsilon_\infty - \frac{\omega_D^2}{\omega\left(\omega + j\gamma_D\right)} - \frac{\Delta\varepsilon.\Omega_L^2}{\left(\omega^2 - \Omega_L^2\right) + j\Gamma_L\omega} \quad (1)$$

where ε_{Au} is the permittivity of dielectric material (gold), ε_∞ is the permittivity at high frequency and its value is 5.9673. The angular frequency can be expressed as $\omega = 2\pi c/\lambda$, c is the velocity of light in vacuum. Moreover, ω_D and γ_D are the plasma frequency and damping frequency respectively, whereas $\Omega_D/2\pi = 2113.6$ THz and $\gamma_D/2\pi = 15.92$ THz. Weighting factor is expressed as $\Delta\varepsilon = 1.09$ while, $\Gamma_L/2\pi = 104.86$ THz and $\Omega_L/2\pi = 650.07$ THz are the spectral width and oscillator strength respectively of the Lorentz oscillators.

The refractive index profile of TiO_2 is calculated by the following equation [32],

$$n^2 = 5.913 + \frac{2.441 \times 10^7}{(\lambda^2 - 0.803 \times 10^7)} \quad (2)$$

Finite-element method (FEM) based commercial COMSOL software was used to investigate the guiding properties and sensing performance of the proposed sensor. Perfectly matched layer (PML) boundary conditions were used to absorb the radiated light towards the surface. Convergence tests were also carried out by optimizing the mesh size and PML thickness, which lead to more accurate results [33]. Proposed sensor computational area was meshed with triangular domain elements 477,497 and boundary domain elements 34,832.

Although, the present study is fully numerical, schematic of a general set-up that can be used for D-shaped PCF SPR sensing is presented in Fig. 1(c). In the proposed system, a wide-band light source like supercontinuum source may use to lunch into the D-shaped PCF and couple to the outer flat surface. An analyte flow channel may consider on top of the gold surface. Analyte sample IN and OUT can be maintained through a pump. Due to interaction between the analyte with ligand, effective index of SPP mode is expected to be changed resulting in a blue or red shift. Finally, the transmitted light can be coupled to an optical spectrum analyzer (OSA) for analysis. The spectrum response can be easily transferred to the computer for better observation.

III. Results and Discussion of D-Shaped PCF SPR Sensor

A. Fabrication of the Proposed D-Shaped PCF

The proposed D-shaped PCF can be fabricated in two methods, (a) indirect method, which is fabricating the PCF in a regular way followed by polishing the upper part of the fiber, and (b) direct method, which is by half-way stacking and controlling the shape of the fiber during the drawing process. In this study, the second method is implemented due to simplicity and not requiring extensive polishing. A prototype of the proposed D-shaped PCF have been fabricated through conventional stack-and-draw method [6], as a scanning electron microscope (SEM) image from the fiber cross-section shown in Fig. 2. The detail of the fabrication process is not within the scope of this study. It should be noted that the imperfection structure in this fiber can be improved in the next fabrications by optimizing fiber drawing parameters. Yet, the light guiding property and confinement loss in a standard microstructured optical fibers strongly depends on the first few air-hole rings. According to the fabricated design, the uniformity in the first few air-hole rings around the fiber core suggests that the fabricated D-shaped PCF would be able to realize the proposed SPR sensor performance.

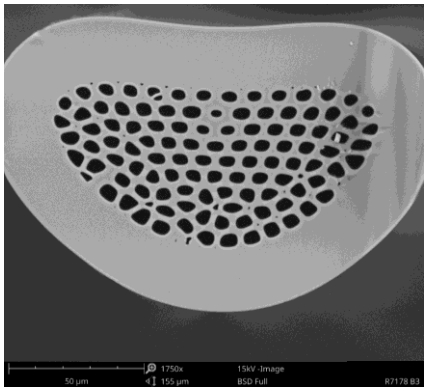

Fig. 2. SEM image of the fabricated D-shaped PCF.

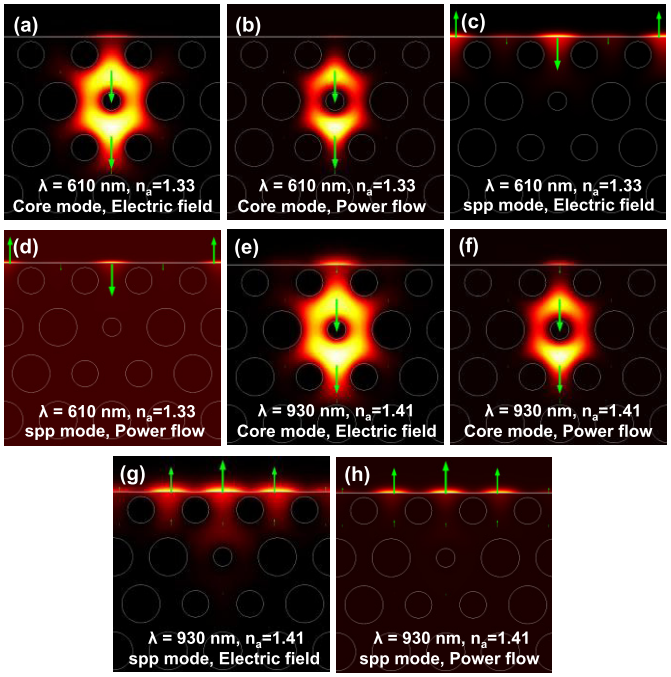

Fig. 3. Electric field and power flow distributions. (a) and (c) Electric field distribution for core and spp mode, respectively at n_a =1.33. (b) and (d) Power flow distribution of core and spp mode, respectively at n_a = 1.33. (e) and (g) Electric field distribution for core and spp mode, respectively, at n_a = 1.41. (f) & (h) Power flow distribution of core and spp mode, respectively at n_a = 1.41.

B. Investigation of the D-shaped PCF SPR Sensor Performance

The evanescent fields produced by propagating light through the core is the key phenomenon of the PCF SPR sensor. The evanescent field excites the metal surface electrons resulting in a surface plasmon wave. Due to the birefringent effect, y-polarized TE mode shows the larger evanescent field resulting in a stronger coupling with the analyte compared to the x-polarized TE mode. Moreover, loss peak appears at the same wavelength for TE^x and TE^y polarization as a result TE^y polarization mode is considered for the following work. Electric field and power distribution of the proposed sensor is shown in Fig. 3.

From Fig. 3, it is clearly visible that core-guided electric field is going towards the dielectric surface/sensing medium.

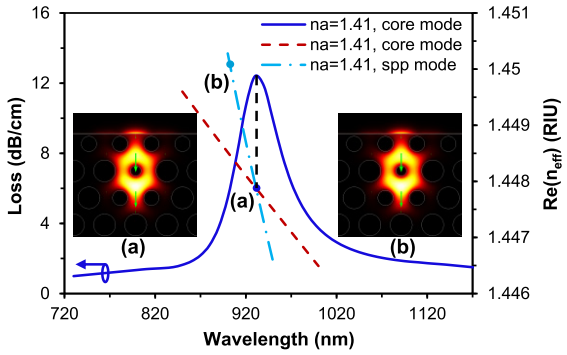

Fig. 4. Dispersion relations of the plasmonic mode (light blue), fundamental core mode (dark read), and loss spectra (blue) with the structural parameters: d_c = 2.3 μm, d_s = 3.28 μm, d = 4.69 μm, t_g = 40 nm, t_t = 5 nm.

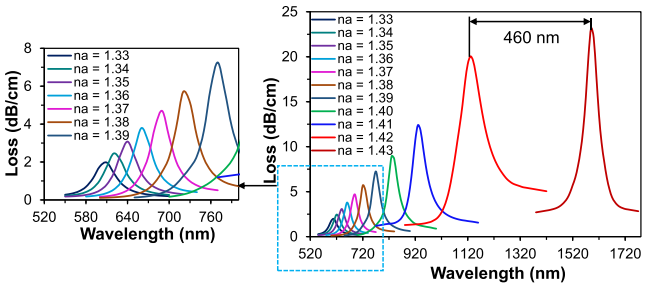

Fig. 5. Loss spectrum with varying analyte RI (n_a) from 1.33-1.43.

Enhancement of field penetration and power distribution on dielectric surface is observed due to the increase of analyte RI; also shifted the resonance peak towards the longer wavelength simultaneously. The maximum presence of field on the dielectric surface indicates the stronger resonance peak which is beneficial for easy detection. Fig. 4 reveals the phase matching condition at 920 nm for analyte RI (n_a) 1.41.

Inset (a) of Fig. 4 shows the core guided fundamental mode, where it indicates the strong field coupling between the core and spp mode resulting in a sharp loss peak. Using the real n_{eff} of core guided mode, loss is calculated from, α *(dB/cm)*$= 8.686\times(2\pi/\lambda).Im(n_{eff})\times 10^4$, where λ is in micron scale. Plasmonic mode is extremely sensitive to the refractive index of dielectric surface. Due to small RI changes of dielectric surface (analyte), RI of plasmonic mode also changes and as a result, phasing matching point changes accordingly. Due to the change of analyte RI from 1.33 to 1.43, loss spectrum are shown in Fig. 5.

According to Fig. 5, with analyte RI 1.33, resonance peak appears at 610 nm where the propagation loss value is 1.97 dB/cm. Generally, PCF based SPR sensors show the high propagation loss which limits the sensor's length to observe it practically. However, proposed D-shaped fiber shows the minimum propagation loss as its core is surrounded by the six rings and only the upper part is polished. Due to low propagation loss, proposed sensor will allow the several centimeters of fiber length to observe the SPR sensor practically, which eliminates the aligning or splicing loss issues. As a result, it will enhance the practical realization of PCF SPR biosensors [3], [18]. Due to the increase of analyte RI from 1.33 to 1.43

TABLE I
PERFORMANCE ANALYSIS BY VARYING ANALYTE RI

Analyte RI	Res. peak wavelength (nm)	Peak loss (dB/cm)	Resonance peak shift (nm)	Sensitivity (nm/RIU)
1.33	610	1.97	10	1,000
1.34	620	2.45	20	2,000
1.35	640	3.07	20	2,000
1.36	660	3.79	30	3,000
1.37	690	4.69	30	3,000
1.38	720	5.69	50	5,000
1.39	770	7.25	60	6,000
1.40	830	8.93	100	10,000
1.41	930	12.39	200	20,000
1.42	1,130	20.05	460	46,000
1.43	1,590	23.18	N/A	N/A

(with iteration of 0.01), resonance wavelength shows the red shift which indicates the phase matching point is also shifted towards the higher wavelength. With the increase of analyte RI, the refractive index difference between the core mode and spp mode decreases significantly, resulting in the dramatic increase of loss value. The proposed sensor shows maximum loss value of 23.13 dB/cm at 1,590 nm wavelength while the analyte RI is 1.43. Higher loss value indicates higher penetration through the cladding region, which means maximum energy transfer from the core-guided mode to spp mode. Due to the change of analyte RI, dramatic change of n_{eff} of the spp mode occurs and phase matching point changes. The proposed sensor also shows the maximum resonance wavelength shift of 460 nm from 1,130 nm to 1,590 nm while the analyte RI changes from 1.42 to 1.43. Usually RI range of biochemical interactions goes from 1.33 (RI of water) up to 1.34/1.35 [34]. However, RI variations between 1.33 and 1.43 is considered based on practical and feasible bio-chemical and chemical sensing [35]. From the WI method, using the maximum wavelength shift of the proposed sensor, shows the sensitivity of 46,000 nm/RIU which is significant for the PCF based SPR type sensors. The WI sensitivity is calculated by following the equation in [25], Sensitivity $S_\lambda(\lambda) = \Delta\lambda_{peak}/\Delta n_a$, where Δn_a is the analyte RI variation and $\Delta\lambda_{peak}$ is the resonant peak shift. The proposed sensor also shows the sensitivities of 1000, 2000, 2000, 3000, 3000, 5000, 6000, 10000, 20000 and 46000 nm/RIU while the analyte RI are 1.33, 1.34, 1.35, 1.36, 1.37, 1.38, 1.39, 1.40, 1.41 and 1.42, respectively as shown in table 1.

It also shows the theoretical maximum sensor resolution of 2.17×10^{-6} RIU (without considering any practical noise influence; and assuming minimum 1% transmitted intensity could be detected); which indicates capability of the sensor in detecting very small RI changes in the order of 10^{-6}, which is better compared to the results reported in [5], [36], and [37].

However, apart from the wavelength interrogation method, amplitude interrogation method was also used to observe the sensor performance. The AI method is less complex and cost effective compared to the WI method as it does not require the wavelength interpolation, whereas only the single wavelength

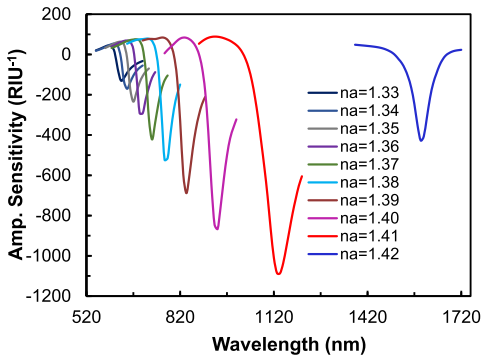

Fig. 6. Dependence of the sensor amplitude sensitivity with the variation of analyte RI.

can detect the analyte [9], [38]. With varying the analyte RI from 1.33 to 1.42, amplitude sensitivity is shown in Fig. 6. Amplitude sensitivity in calculated according to the following equation [38],

$$S_A(\lambda)[RIU^{-1}] = -\frac{1}{\alpha(\lambda, n_a)}\frac{\partial\alpha(\lambda, n_a)}{\partial n_a} \quad (3)$$

where α (λ, n_a) is the overall loss where RI is equal to n_a and $\partial\alpha$ (λ, n_a) is the loss difference of two loss spectra due two adjacent analyte RI.

According to Fig. 6, proposed sensor shows the maximum amplitude sensitivity of 1,086 RIU^{-1} at wavelength 1,140 nm while the analyte RI is 1.42. Amplitude sensitivity increases dramatically with the increase of analyte RI from 1.33 to 1.41, except analyte RI 1.42. At analyte RI 1.43, loss difference between the adjacent loss spectrum due to analyte RI 1.42 and 1.43 is less and the overall loss value is higher at analyte RI 1.42. As a result, it shows the lower amplitude sensitivity. The proposed sensor shows the amplitude sensitivities of 129, 170, 234, 292, 422, 522, 689, 867, 1086 and 427 while the analyte RI are 1.33, 1.34, 135, 1.36, 1.37, 1.38, 1.39, 1.40, 1.41 and 1.42, respectively. Additionally, according to the AI method proposed sensor shows the theoretical maximum refractive index resolution of 9.28×10^{-6} (without considering any practical noise influence; assuming that sensor could detect minimum 1% change of the transmission intensity), which is maximum compared to the reported in [15], [25], and [37]. However, proposed sensor shows the minimum sensing performance in the sensing range of 1.33-1.35. It shows the wavelength sensitivity of 1000, 2000 and 2000 nm/ RIU and the amplitude sensitivity of 129, 170 and 234 RIU^{-1} with respect to the analyte RI of 1.33, 1.34 and 1.35, respectively. These results are comparable with the reported in [15] and [21], with simple PCF SPR sensor structure and minimum propagation loss. The analyte RI range of 1.33-1.35, proposed sensor shows the sensor resolution in order of 10^{-5}, which is comparable with the reported references in [21], [28], and [40]. Due to minimum propagation loss, this minimum sensitivity with the sensor resolution will be satisfactory to detect the biochemical. The performance comparisons of the reported sensors with the proposed sensor are shown in table 2. Besides the analyte RI effect, plasmonic material gold layer

TABLE II
PERFORMANCE COMPARISON OF THE REPORTED SPR SENSORS

Characteristics	Wavelength (nm)	RI Range	Interrogation method	Sensitivity	Resolution (RIU)	Loss (dB/cm)	Ref.
ITO based D-shaped SPR sensor	1870-2300	1.33-1.38	Wavelength	17,000 nm/RIU	5.8×10^{-6}	38	[5]
			Amplitude	74 RIU^{-1}	1.3×10^{-5}		
Multichannel PCF	550-950	1.33-1.39	Wavelength	4,600 nm/RIU	2×10^{-5}	78	[10]
Hollow-core silver-nanowires	560-610	1.1-1.6	Wavelength	14,240 nm/RIU	N/A	N/A	[12]
Exposed-core grapefruit fiber	460-1120	1.33-1.42	Wavelength	13,500 nm/RIU	N/A	80	[13]
Graphene based D-shaped fiber	480-650	1.33-1.37	Wavelength	3,700 nm/RIU	2.7×10^{-5}	167	[18]
			Amplitude	216 RIU^{-1}	4.6×10^{-5}		
Scaled down hollow-core D-shaped fiber	550-750	1.33-1.34	Wavelength	2,900 nm/RIU	N/A	1,950	[19]
			Amplitude	120 RIU^{-1}	N/A		
Hollow core D-shaped PCF	650-850	1.32-1.36	Wavelength	6,430 nm/RIU	N/A	N/A	[20]
MCFF based SPR sensor	1000-1400	1.46-1.468	Wavelength	23,000 nm/RIU	4.3×10^{-6}	695	[25]
			Amplitude	820 RIU^{-1}	1.2×10^{-5}		
Solid core honeycomb PCF SPR sensor	940-1040	1.32-1.322	Wavelength	13,750	7.2×10^{-6}	170	[38]
			Amplitude	400	2.5×10^{-5}		
Two microfluidic slots	500-800	1.33-1.34	Wavelength	N/A	6×10^{-5}	210	[39]
			Amplitude	N/A	4×10^{-5}		
Proposed D-shaped PCF SPR	550-1770	1.33-1.43	Wavelength	46,000 nm/RIU	2.2×10^{-6}	1.97	(Proposed)
			Amplitude	1,086 RIU^{-1}	9.2×10^{-6}		

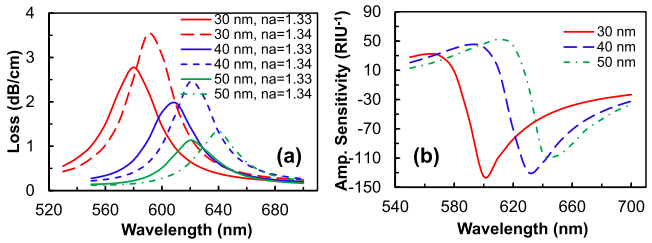

Fig. 7. Gold thickness variation from 30-50 nm. (a) Loss spectrum. (b) Amplitude sensitivity ($n_a = 1.33$); by setting $h = 8\ \mu$m,$d_c = 2.3\ \mu$m, $d_s = 3.28\ \mu$m, $d = 4.69\ \mu$m, $t_t = 5$ nm.

has significant effects on SPR sensing. Gold is chemically stable in various environments such as aqueous, water and shows the higher resonance shift [16].

By varying the Au thickness from 30 to 50 nm, loss spectrum and amplitude sensitivity effects are shown in Fig. 7. According to Fig. 7(a), at Au thickness 30 nm, maximum loss peak value 2.8 dB/cm is achieved at resonance wavelength 580 nm while the analyte RI 1.33 and resonance wavelength shifted to 590 nm with increment of loss value of 3.52 dB/cm at analyte RI 1.34. Loss value decreases with the increase of Au thickness and the minimum loss value 1.13 dB/cm is achieved at 50 nm Au thickness while the analyte RI 1.33. However, at analyte 1.33, the proposed sensor shows the wavelength sensitivity of 1000, 1000 and 2000 nm/RIU, while the Au thicknesses are 30, 40 and 50 nm, respectively. Although it shows the high sensitivity at 50 nm, the signal to noise ratio is low and resonance spectrum is broad which may give the false positive response. Thicker Au layer introduces higher damping loss of gold layer. As a result, the evanescent field penetration towards the sample decreases [16]. Also, the presence of surface plasmons on the sensing medium is decreased dramatically. However, with the change of Au thickness, the resonance peak also changes according to this phenomena and can be applied for monitoring the nanoparticles concentration on the Au surface. Furthermore, amplitude sensitivity also decreases with the increase of gold thickness as shown in Fig. 7(b).

The proposed sensor shows the maximum amplitude sensitivity of 135 RIU^{-1} at wavelength 630 nm while the Au thickness is 30 nm. This amplitude sensitivity decreases to 129 and 107 RIU^{-1} when the Au thickness increases to 40 and 50 nm, respectively. By considering the optimum loss value, signal to noise ratio and the adjustment of Au thickness with the other parameters, Au thickness is optimized with 40 nm. Practically, gold material cannot stick with the glass surface (silica PCF). As a result, a very thin TiO_2 layer is used as an adhesive layer. TiO_2 has a broad wavelength range of transparent property. As a result, TiO_2 will not disrupt the light penetration significantly [25]. Its refractive index is also high, which allows to tune the sensor's operating wavelength from visible to near IR region [11]. By varying the TiO_2 layer, loss spectrum and amplitude sensitivity responses are shown in Fig. 8. According to Fig. 8(a), it is clearly visible that without TiO_2 layer, core-guided mode penetrates more and coupled with the spp mode which results in the high loss propagation loss 2.2 dB/cm at $n_a = 1.33$.

The propagation loss gradually decreases to 1.9 dB/cm and 1.8 dB/cm when the TiO_2 layer thickness increases 5 and 10 nm, respectively. Thicker surface layer will hamper the light coupled between the core mode and spp mode. The same scenario was also observed for amplitude sensitivity in Fig. 8(b). With the increase of the TiO_2 layer thickness, amplitude sensitivity decreased gradually. Maximum sensitivity 136 RIU^{-1} was observed when $t_t = 0$ nm. Amplitude sensitivity gradually decreased to 129 and 120 RIU^{-1} with the TiO_2 thickness of 5 and 10 nm, respectively.

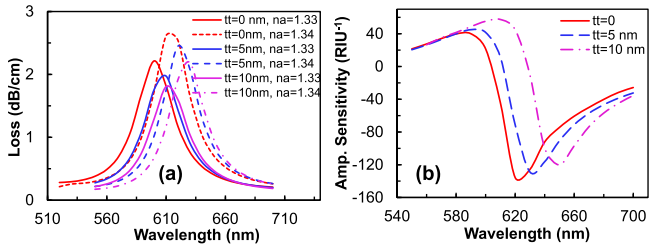

Fig. 8. TiO_2 thickness variation from 0-10 nm. (a) Loss spectrum. (b) Amplitude sensitivity ($n_a = 1.33$); by setting $d_c = 2.3$ μm, $d_s = 3.28$ μm, $d = 4.69$ μm, $t_g = 40$ nm.

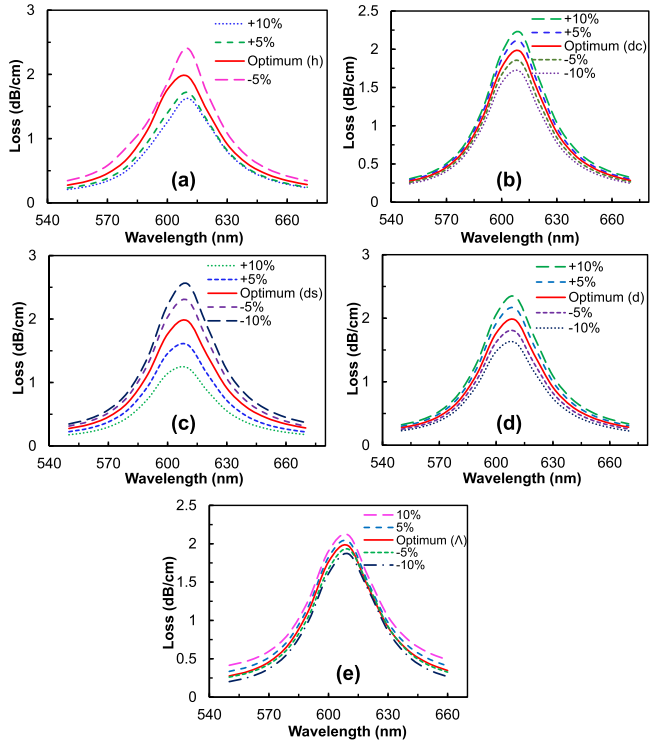

Fig. 9. Fabrication tolerance investigation. Loss spectrum is a function of wavelength with varying: (a) polishing depth, h; (b) central air-hole, d_c; (c) scaled down air-hole, d_s; (d) standard air-holes, d; and (e) pitch, Λ.

Furthermore, the fabrication tolerance of the proposed sensor is investigated by considering the optimum parameters, $h = 8$ μm, $d_c = 2.3$ μm, $d_s = 3.28$ μm, $d = 4.69$ μm and $\Lambda = 6.73$ μm, shown in Fig 9. Fig. 9(a) shows the polishing depth effect of the proposed sensor which indicates resonance peaks due to the change of polishing depth, which appear at the same wavelength 610 nm with different loss values. By decreasing the 5% polishing from the optimum polishing height, showed increased loss value of 2.4 dB/cm where the optimum loss value was 1.97 dB/cm. This scenario is due to short path distance between the core and metal surface which can ensure the strong mode coupling. In contrast, increasing the polishing depth leads to the weaker coupling between the core-mode and spp mode. As a result, lower loss value is found. In addition, the polishing depth and small central air-hole d_c were important parameters, which helped to establish the phase matching phenomena shown in Fig. 9(b). According to Fig. 9(b), due to the reduction of the diameter d_c, light is more concentrated through the core resulting in a reduction of field penetration. On the contrary, loss values increase with the increase of diameter d_c which indicates the stronger coupling of core mode and spp mode. However, larger diameter of d_c disrupts the concentration of light through the core. It spreads the core-guided light towards the cladding region which diminishes the sensor performance. Furthermore, the effects of loss spectrum while varying the scaling down air-hole diameter d_s is shown in Fig. 9(c). Increasing the diameter d_s reduces the field penetration gap and increases the distance between the core and gold surface. As a result, the loss value decreases. The opposite scenario was found for the decrease of diameter d_s where the loss was increased to 2.56 dB/cm at 10% decrease of the optimum air-hole diameter d_s. Fig. 9(d) shows, by varying the cladding air-holes d, loss peaks maintain the resonant wavelength 610 nm. Due to the increase of air-hole diameter d, the gap between two air-holes reduced.

As a result, the loss depth decreased. In contrast, loss increased from optimum 1.97 dB/cm to 2.34 dB/cm with 10% reduction of cladding air holes diameter. The same scenario was also observed for the pitch size, Λ variation shown in Fig. 9(e). Due to the increase of pitch size, the gap between two air-holes increased, resulting in an increase in loss. The increase of loss was 2.11 dB/cm while the Λ was increased to 10%. On the contrary, reducing the Λ size brings the air holes closer and prevents the penetration through the cladding core resulting in a reduction of loss.

According to the above discussion, it was found that due to the variation of $\pm$10% of the proposed PCF parameters, sensors shows the very low loss variations and maintains the constant resonant wavelength at 620 nm. The main advantage of the proposed D-shaped PCF SPR is having high sensitivity compare to other types of SPRs. Also, its sensing area can be scalable due to its large flat surface. Additionally, its functionality and flexibility of the proposed structure with having high RI fluids, open up many opportunities for designing versatile SPR sensors, based on this hybrid format of waveguide. The structure of D-shaped PCF combines the advantages of PCF with the multi-functionality of planar waveguides. Due to its flat surface, smoother surfaces can be achieved after the deposition of metal. Finally, owing to its outer metal layer, an unknown analyte concentration could be detected by fluid flow through the metallic surface.

IV. Conclusion

In summary, a D-shaped PCF SPR sensor is proposed and numerically investigated using full-vectorial FEM method. Incorporating plasmonic Au and TiO_2 thin layers top of the flat surface of the D-shaped PCF, the highest sensitivity of the proposed sensor could be realized. The wavelength and amplitude sensitivity as high as 46,000 nm/RIU and 1,086 RIU^{-1} has been demonstrated with the theoretical maximum sensor resolution of 2.2×10^{-6} and 9.2×10^{-6} RIU, respectively. The modelled sensor gives the minimum propagation loss of 1.97 dB/cm at $n_a = 1.33$, which paves the practical realization of PCF SPR biosensors. The results demonstrate the feasibility of D-shaped based SPR sensor towards the

possibility of an integrated SPR sensor as a lab-on-a-fiber technology for the real time diagnostics purpose such as glucose monitoring, biochemicals or chemicals detection.

ACKNOWLEDGMENT

Authors thank ILRG fabrication team for help to fabricate the fiber.

REFERENCES

[1] X. Fan and I. M. White, "Optofluidic microsystems for chemical and biological analysis," *Nature Photon.*, vol. 5, no. 10, pp. 591–597, 2011.
[2] A. Ricciardi, M. Consales, G. Quero, A. Crescitelli, E. Esposito, and A. Cusano, "Versatile optical fiber nanoprobes: From plasmonic biosensors to polarization-sensitive devices," *ACS Photon.*, vol. 1, no. 1, pp. 69–78, 2013.
[3] A. A. Rifat *et al.*, "Photonic crystal fiber based plasmonic sensors," *Sens. Actuators B, Chem.*, vol. 243, pp. 311–325, May 2017.
[4] G. Robinson, "The commercial development of planar optical biosensors," *Sens. Actuators B, Chem.*, vol. 29, nos. 1–3, pp. 31–36, 1995.
[5] J. N. Dash and R. Jha, "Highly sensitive side-polished birefringent PCF-based SPR sensor in near IR," *Plasmonics*, vol. 11, pp. 1–5, Dec. 2016.
[6] G. A. Mahdiraji *et al.*, "Challenges and solutions in fabrication of silica-based photonic crystal fibers: An experimental study," *Fiber Integr. Opt.*, vol. 33, nos. 1–2, pp. 85–104, 2014.
[7] R. Ahmmed, R. Ahmed, and S. A. Razzak, "Design of large negative dispersion and modal analysis for hexagonal, square, FCC and BCC photonic crystal fibers," in *Proc. Int. Conf. Informat., Electron. Vis. (ICIEV)*, 2013, pp. 1–6.
[8] R. Ahmed, M. M. Khan, R. Ahmmed, and A. Ahad, "Design, simulation & optimization of 2D photonic crystal power splitter," *Opt. Photon. J.*, vol. 3, p. 13, Mar. 2013.
[9] A. A. Rifat, G. Mahdiraji, D. Chow, Y. Shee, R. Ahmed, and F. Adikan, "Photonic crystal fiber-based surface plasmon resonance sensor with selective analyte channels and graphene-silver deposited core," *Sensors*, vol. 15, no. 5, pp. 11499–11510, Mar. 2015.
[10] R. Otupiri, E. Akowuah, and S. Haxha, "Multi-channel SPR biosensor based on PCF for multi-analyte sensing applications," *Opt. Exp.*, vol. 23, no. 12, pp. 15716–15727, 2015.
[11] D. Gao, C. Guan, Y. Wen, X. Zhong, and L. Yuan, "Multi-hole fiber based surface plasmon resonance sensor operated at near-infrared wavelengths," *Opt. Commun.*, vol. 313, pp. 94–98, Feb. 2014.
[12] Y. Lu, X. Yang, M. Wang, and J. Yao, "Surface plasmon resonance sensor based on hollow-core PCFs filled with silver nanowires," *Electron. Lett.*, vol. 51, no. 21, pp. 1675–1677, 2015.
[13] X. Yang, Y. Lu, M. Wang, and J. Yao, "An exposed-core grapefruit fibers based surface plasmon resonance sensor," *Sensors*, vol. 15, no. 7, pp. 17106–17114, Jul. 2015.
[14] T. Biswas, R. Chattopadhyay, and S. K. Bhadra, "Plasmonic hollow-core photonic band gap fiber for efficient sensing of biofluids," *J. Opt.*, vol. 16, no. 4, p. 045001, 2014.
[15] S. I. Azzam, M. F. O. Hameed, R. E. A. Shehata, A. Heikal, and S. Obayya, "Multichannel photonic crystal fiber surface plasmon resonance based sensor," *Opt. Quant. Electron.*, vol. 48, pp. 1–11, Feb. 2016.
[16] A. A. Rifat *et al.*, "Surface plasmon resonance photonic crystal fiber biosensor: A practical sensing approach," *IEEE Photon. Technol. Lett.*, vol. 27, no. 15, pp. 1628–1631, Aug. 1, 2015.
[17] A. A. Rifat *et al.*, "Copper-graphene-based photonic crystal fiber plasmonic biosensor," *IEEE Photon. J.*, vol. 8, no. 1, pp. 1–8, Feb. 2016.
[18] J. N. Dash and R. Jha, "On the performance of graphene-based D-shaped photonic crystal fibre biosensor using surface plasmon resonance," *Plasmonics*, vol. 10, pp. 1123–1131, Mar. 2015.
[19] N. Luan, R. Wang, W. Lv, and J. Yao, "Surface plasmon resonance sensor based on D-shaped microstructured optical fiber with hollow core," *Opt. Exp.*, vol. 23, no. 7, pp. 8576–8582, Mar. 2015.
[20] Z. Tan, X. Li, Y. Chen, and P. Fan, "Improving the sensitivity of fiber surface plasmon resonance sensor by filling liquid in a hollow core photonic crystal fiber," *Plasmonics*, vol. 9, pp. 167–173, Jun. 2014.
[21] J. N. Dash and R. Jha, "Graphene-based birefringent photonic crystal fiber sensor using surface plasmon resonance," *IEEE Photon. Technol. Lett.*, vol. 26, no. 11, pp. 1092–1095, Jun. 1, 2014.
[22] J. Boehm, A. François, H. Ebendorff-Heidepriem, and T. M. Monro, "Chemical deposition of silver for the fabrication of surface plasmon microstructured optical fibre sensors," *Plasmonics*, vol. 6, pp. 133–136, Mar. 2011.
[23] N. Takeyasu, T. Tanaka, and S. Kawata, "Metal deposition deep into microstructure by electroless plating," *Jpn. J. Appl. Phys.*, vol. 44, p. L1134, Aug. 2005.
[24] P. J. A. Sazio *et al.*, "Microstructured optical fibers as high-pressure microfluidic reactors," *Science*, vol. 311, no. 5767, pp. 1583–1586, 2006.
[25] A. A. Rifat, G. Mahdiraji, Y. M. Sua, R. Ahmed, Y. Shee, and F. M. Adikan, "Highly sensitive multi-core flat fiber surface plasmon resonance refractive index sensor," *Opt. Exp.*, vol. 24, no. 3, pp. 2485–2495, 2016.
[26] M. Tian, P. Lu, L. Chen, C. Lv, and D. Liu, "All-solid D-shaped photonic fiber sensor based on surface plasmon resonance," *Opt. Commun.*, vol. 285, no. 6, pp. 1550–1554, Mar. 2011.
[27] Z. Tan, X. Hao, Y. Shao, Y. Chen, X. Li, and P. Fan, "Phase modulation and structural effects in a D-shaped all-solid photonic crystal fiber surface plasmon resonance sensor," *Opt. Exp.*, vol. 22, no. 12, pp. 15049–15063, Jun. 2014.
[28] L. Peng, F. Shi, G. Zhou, S. Ge, Z. Hou, and C. Xia, "A surface plasmon biosensor based on a D-shaped microstructured optical fiber with rectangular lattice," *IEEE Photon. J.*, vol. 7, no. 5, pp. 1–9, Oct. 2015.
[29] G. Wang *et al.*, "Highly sensitive D-shaped photonic crystal fiber biological sensors based on surface plasmon resonance," *Opt. Quant. Electro.*, vol. 48, pp. 1–9, Jan. 2016.
[30] R. Ziblat, V. Lirtsman, D. Davidov, and B. Aroeti, "Infrared surface plasmon resonance: A novel tool for real time sensing of variations in living cells," *Biophys. J.*, vol. 90, no. 7, pp. 2592–2599, 2006.
[31] A. Vial, A.-S. Grimault, D. Macías, D. Barchiesi, and M. L. de la Chapelle, "Improved analytical fit of gold dispersion: Application to the modeling of extinction spectra with a finite-difference time-domain method," *Phys. Rev. B*, vol. 71, p. 085416, Feb. 2005.
[32] J. R. DeVore, "Refractive indices of rutile and sphalerite," *J. Opt. Soc. Amer.*, vol. 41, no. 6, pp. 416–417, 1951.
[33] R. Ahmed, A. A. Rifat, A. K. Yetisen, Q. Dai, S. H. Yun, and H. Butt, "Multiwall carbon nanotube microcavity arrays," *J. Appl. Phys.*, vol. 119, p. 113105, Mar. 2016.
[34] A. Aray *et al.*, "SPR-based plastic optical fibre biosensor for the detection of C-reactive protein in serum," *J. Biophoton.*, vol. 9, no. 10, pp. 1077–1084, 2016.
[35] A. K. Yetisen *et al.*, "Color-selective 2.5D holograms on large-area flexible substrates for sensing and multilevel security," *Adv. Opt. Mat.*, vol. 4, no. 10, pp. 1589–1600, 2016.
[36] M. Piliarik, J. Homola, Z. Maníková, and J. Čtyroký, "Surface plasmon resonance sensor based on a single-mode polarization-maintaining optical fiber," *Sens. Actuators B, Chem.*, vol. 90, pp. 236–242, Apr. 2003.
[37] F. Chiavaioli *et al.*, "Sol–gel-based titania–silica thin film overlay for long period fiber grating-based biosensors," *Anal. Chem.*, vol. 87, no. 24, pp. 12024–12031, 2015.
[38] B. Gauvreau, A. Hassani, M. Fassi Fehri, A. Kabashin, and M. A. Skorobogatiy, "Photonic bandgap fiber-based surface plasmon resonance sensors," *Opt. Exp.*, vol. 15, no. 18, pp. 11413–11426, 2007.
[39] R. Otupiri, E. Akowuah, S. Haxha, H. Ademgil, F. A. Malek, and A. Aggoun, "A novel birefrigent photonic crystal fiber surface plasmon resonance biosensor," *IEEE Photon. J.*, vol. 6, no. 4, pp. 1–11, Aug. 2014.
[40] A. A. Rifat, G. A. Mahdiraji, Y. Shee, M. J. Shawon, and F. M. Adikan, "A novel photonic crystal fiber biosensor using surface plasmon resonance," in *Proc. Eng.*, vol. 140, 2016, pp. 1–7.

Ahmmed A. Rifat, photograph and biography not available at the time of publication.

Rajib Ahmed, photograph and biography not available at the time of publication.

G. Amouzad Mahdiraji, photograph and biography not available at the time of publication.

F. R. Mahamd Adikan, photograph and biography not available at the time of publication.